View Online / Journal Homepage
Dynamic Article Links

Lab on a Chip

Cite this: DOI: 10.1039/c2lc40275k

www.rsc.org/loc

PAPER

Lab-in-a-tube: on-chip integration of glass optofluidic ring resonators for label-free sensing applications†

Stefan M. Harazim,*[a] Vladimir A. Bolaños Quiñones,[a] Suwit Kiravittaya,[a] Samuel Sanchez*[a] and Oliver G. Schmidt[ab]

Received 19th March 2012, Accepted 14th May 2012
DOI: 10.1039/c2lc40275k

The fabrication of tubular rolled-up optofluidic ring resonators (RU-OFRRs) based on glass (SiO_2) material with high quality factors is reported. A novel methodology combining lab-on-a-chip fabrication methods and rolled-up nanotech is presented for the fabrication of fully integrated tubular optofluidic sensors. The microfluidic integration of several RU-OFRRs on one chip is solved by enclosing the microtubes with a patterned robust SU-8 polymeric matrix. A viewport on each microtube enables exact excitation and monitoring of whispering gallery modes with a photoluminescence spectroscopy system under constant ambient conditions, while exchanging the content of the RU-OFRR with liquids of different refractive indices. The refractrometric sensor capabilities are investigated regarding signal stability, sensitivity and reliability. The sensitivity of the integrated RU-OFRR, which is the response of the modes to the change in refractive index of the liquid, is up to 880 nm/refractive index units (RIU).

Introduction

Label-free optofluidic sensor technology is a topic of great interest ranging from analytical science to the pharmaceutical industry, with a variety of applications implemented as lab-on-a-chip (LoC) devices.[1–6] Part of optofluidics merges microfluidics with optical sensing capabilities into a single device. Refractive index (RI) based sensors can be sensitive to both RI changes in the bulk medium and on the sensor surface, and are realized by different approaches such as interferometry,[7] surface plasmon[8] and optical resonances.[1,3,4,9] Optical resonators come in different shapes,[10–12] and if combined with fluidics they are named optofluidic ring resonators (OFRRs). Only in tubular geometry they do inherently combine compact and practical fluidic functionality with optical sensitivity.[3,4,9] According to the resonant conditions, circulating light can interfere constructively at certain frequencies called whispering gallery modes (WGMs) whose evanescent field decays exponentially outside the tubular wall. The sensing mechanism of OFRRs is the response of the evanescent field to changes in the RI near the surface of the tubular wall. The quality-factor (Q) of such ring resonators, related to the linewidth of WGMs in the detected light spectrum, is an indicator of the quality of the fabricated optical device. High quality factors are preferable in order to work efficiently as label-free bio-sensors for cells,[13] bio-analytes[2,4,9,14] and vapours.[5,15]

Liquid core optical ring resonators (LCORRs) are part of the OFRR family and often rely on the fabrication of narrow circular channels by glass capillary pulling.[13,16] Although this kind of OFRR provides very high quality factors (*e.g.* 10^6), it is not suited for parallel microfluidic on-chip integration due to its fabrication technique, large dimensions and fragility. Other members of the OFRR family are liquid-core microtube optical ring resonators (LCMORs)[4] and rolled-up micro cavity ring resonators (RU-μCRRs),[9] both are based on rolled-up nanotechnology,[4,9,17,18] but which up to now have shown relatively low Q values, in the range of several hundreds.[4,9,13] However, using this technology, large arrays of tubular fluidic channels with a well-defined shape and size can be fabricated on virtually any kind of substrate.[9,13,19,20] Due to their easy size tuneability,[18] they perfectly match the typical dimensions of microfluidic channels, both in length and diameter, and thus are good candidates for inclusion in compact LoC systems. First steps towards the integration of rolled-up microtubes into microfluidic systems have been reported previously[21,22] but their optofluidic functionality after microfluidic integration remains unexplored.

Here, we report the fabrication and characterization of high Q rolled-up optofluidic ring resonators, fully integrated into lab-on-a-chip devices. The ring resonators are fabricated on a mother substrate and consist of rolled-up glass (SiO_2) microtubes with diameters close to 10 μm. Selected microtubes can be picked up from the mother substrate and transferred to the target microchip for further assembly. Optical characterization by photoluminescence (PL) spectroscopy reveals high Q values of up to 2900. We describe a technology platform for the integration process from the fabrication of RU-OFRRs to the

[a]*Institute for Integrative Nanosciences, IFW Dresden, Helmholtzstr. 20, D01069 Dresden, Germany. E-mail: s.harazim@ifw-dresden.de; s.sanchez@ifw-dresden.de*
[b]*Material Systems for Nanoelectronics, Chemnitz University of Technology, Reichenhainer Str. 70, 09107 Chemnitz, Germany*
† Electronic Supplementary Information (ESI) available. See DOI: 10.1039/c2lc40275k/

final device. The stability of the response signal and the reproducibility are evaluated by allowing different analytes to flow through the devices for defined periods of time. We obtain a minimum detection limit of 3.4×10^{-4} per refractive index unit (RIU) and a maximum sensitivity of 880 nm RIU^{-1}, which is the highest value measured for any RU-OFRR to date.

Materials and methods

The final chip device pictured in Fig. 1a consists of a microfluidic channel system (Fig. 1b) where the in- and outlets are bridged by integrated rolled-up microtubes. The optical quality of the RU-OFFRs is evaluated by PL spectroscopy in a wavelength range from visible to near infrared (Fig. 1c). Each of the six main fabrication steps is displayed and briefly described in Fig. 1.

Step 1: Preparation of the target substrate

A square shaped glass plate (D263T, Siegert Consulting e.K., Germany) with a thickness of 500 μm and a side length of 22 mm was selected as the substrate, providing optical transmission of over 90% in the required wavelength range from 400 to 800 nm.

The four white squares shown in Fig. 1b allow for optical alignment on the sample. These squares were fabricated onto the glass by using the lift-off photoresist AZ-5214E (Microchemicals GmbH, Germany) patterned by photolithography followed by the deposition of 10 nm Cr by electron beam (e-beam) evaporation (BOC Edwards FL400, Germany). A two-step photolithography process was carried out to fabricate the supporting structures which hold and elevate the microtubes. The first step involved the deposition of negative photoresist SU-8 10 (MicroChem, MA, USA), which was spin coated at 5000 rpm to produce a 5 μm thick support structure onto the substrate. The pattern for this support structure was transferred to the photoresist with a mask aligner (MA56, SÜSS MicroTec AG, Germany) in contact mode and a Cr photomask by UV-light exposure at a wavelength of 365 nm. The second SU-8 10 layer was spin-coated at 2000 rpm to fabricate a 15 μm thick resist layer. The patterning of this second layer results in an alignment structure on the first photoresist layer. Both structured layers together form a so-called socket. The resist development and baking times were performed with an additional thermal cross-linking step[23] at 180 °C on a hotplate for 10 min for each SU-8 layer separately.

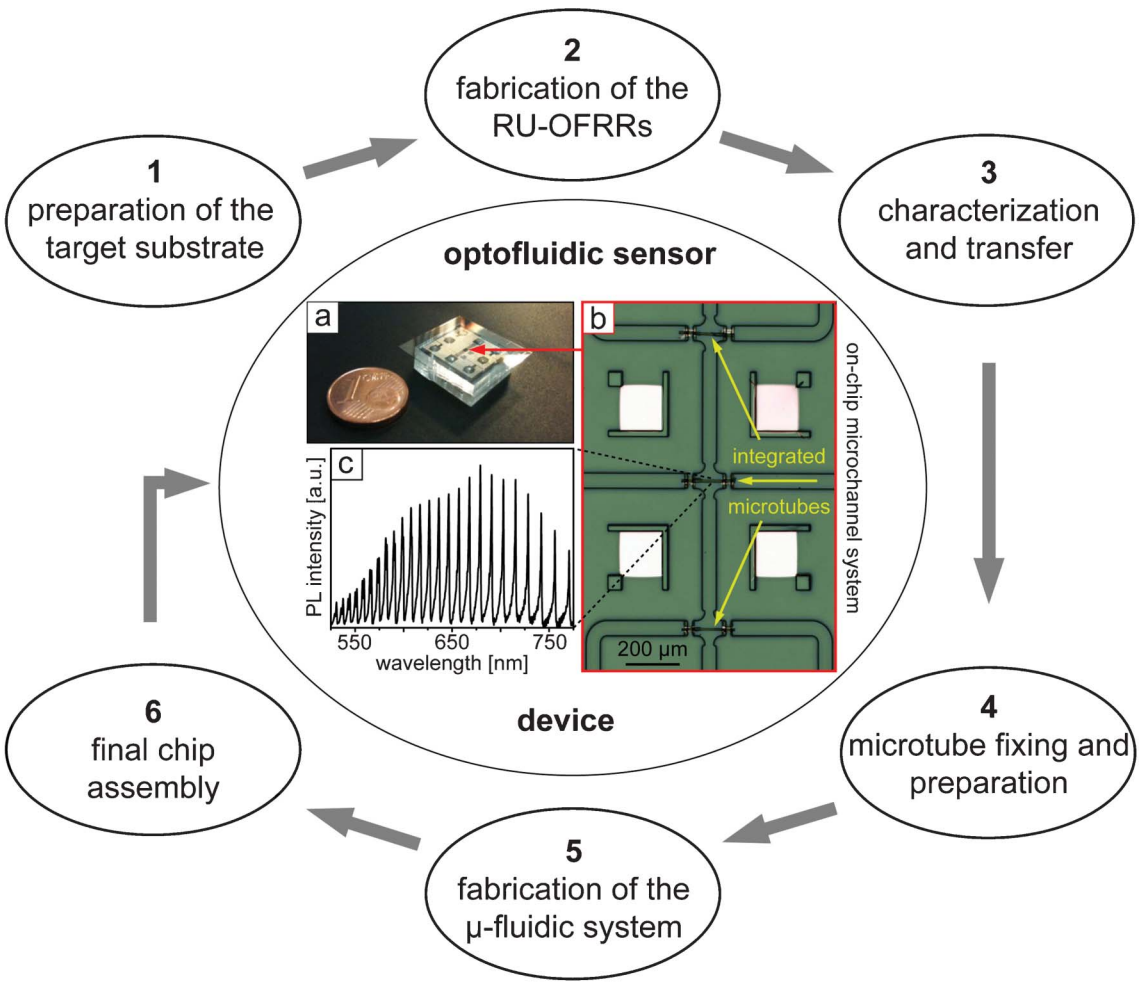

Fig. 1 Fabrication process flowchart for the integration of high quality rolled-up optofluidic resonators. (a) Photograph of a fabricated optofluidic sensing chip device. (b) Optical microscope image of three microtubes integrated into a microchannel system. (c) Background subtracted PL spectrum measured on a microtube integrated into the optofluidic chip sensor.

Step 2: Fabrication of the rolled-up optofluidic ring resonators

The fabrication of tubular optofluidic ring resonators was carried out by rolled-up nanotech on polymer.[19,20,24] In brief, a 2.4 μm thick photoresist pattern was spin coated at a speed of 3500 rpm onto a Si mother substrate using the positive photoresist ARP-3510 (Allresist GmbH, Germany). The deposition of two thin SiO_2 layers on this pattern was performed by tilted e-beam deposition[24] at different deposition rates, generating a highly pre-strained SiO_2/SiO_2 nanomembrane on the surface. The deposited thicknesses were 10 nm (at 1.5 nm s^{-1}) SiO_2 and 60 nm (at 0.05 nm s^{-1}) SiO_2, respectively. The roll-up of the deposited membranes was performed by selectively dissolving the underlying sacrificial polymer layer with acetone. Afterwards, the acetone was replaced by liquid CO_2 in a critical point dryer (CPD). The final Si-substrate (10 × 10 mm^2) contained about 400 RU-OFRRs with diameters of about 10 μm.

Step 3: Resonator characterization and transfer of microtubes

The optical characterization of the rolled-up microtubes was carried out with a micro PL system (Renishaw™) containing a HeCd laser at 442 nm and a charge-coupled device sensor. Each RU-OFRR was measured in order to obtain information about the optical resonance spectrum of each microtube. Based on this screening procedure, a set of high quality microtubes was selected and transferred by micro-manipulation to the SU-8 sockets on the target substrate prepared in step 1.

Step 4: Microtube fixing and preparation

The transferred microtubes were fixed to the sockets by deposition of a thin layer of Al_2O_3 by atomic layer deposition (ALD, Savannah™ 100, CambridgeNanoTech Inc.). The ALD deposition was performed using trimethylaluminium (TMA, Sigma Aldrich) and deionized (DI) water as precursors at 150 °C, obtaining 10 nm Al_2O_3 deposited inside and outside the tubular wall. Ultraviolet (UV) light protector caps were deposited at the place where the microtube is supported by the sockets. The protectors were fabricated by photolithography lift-off using the photoresist AZ-2070 nlof (Microchemicals GmbH, Germany) and e-beam evaporation of $Cr/Au/Cr/SiO_2$ (5/50/5/10 nm) at 0.05 nm s^{-1}. The lift-off process was done in dimethylsulfoxide (DMSO) at 50 °C over 10 min. The sample was cleaned in DI water.

Step 5: Fabrication of the microchannel system

The microfluidic channel system was defined by negative photoresist SU-8 10. The resist was spin coated at 1500 rpm onto the sample to realize a channel with a height of 20 μm. Patterning was performed by UV light photolithography. To prevent swelling of the resist upon contact with fluid a final thermal cross-linking step was performed at 180 °C over 10 min.[23]

Step 6: Final chip assembly

A polydimethylsiloxane (PDMS, Sylgard 184 Silicone Elastomer KIT, Dow Corning, MI, USA) mixture (1 : 10) was freshly prepared and poured into an Al frame (15 × 15 mm^2 side length, 5 mm height) on a blank Si wafer and cured for 20 min at 100 °C on a hotplate. After peeling off the PDMS from the Si wafer, the in- and outlets in the PDMS to the microfluidic system were defined by drilling pin holes with a cutting needle matching the position of the inlets in the microchannel system on the target substrate. A coupling layer of 4 nm SiO_2 was deposited by e-beam evaporation at 0.05 nm s^{-1} on top of the SU-8 10 from step 5. The final assembly was carried out after oxygen plasma treatment of the substrate surfaces and the PDMS for 30 s at 30 W. The holes of the PDMS were accurately aligned with the inlets and the lid was gently pressed onto the substrate to establish permanent and firm bonding. After each fabrication step the optical quality of the microtubes was carefully checked to confirm that the fabrication techniques did not harm the optical quality of the RU-OFRRs.

Optofluidic setup

A pulsation free syringe pump system (neMESYS, Cetoni GmbH, Germany) was employed to pump the liquids into the device and through the microfluidic structures. The syringes (250 μl) were connected to the chip *via* polytetrafluoroethylene (PTFE) tubing with an outer diameter of 0.9 mm, which was simply plugged into the corresponding inlet pin holes of the PDMS. The pumping velocity can be tuned between 0 to 2 μl min^{-1} by software. The sensor chip-device was then mounted onto a PL system with a spectral resolution of 0.02 nm.

Utilized liquids

Liquids with slightly different refractive index values were chosen as shown in Table 1. DI water is used as a blank, which is modified with different solutions at different concentrations, such as glucose or phosphate buffered saline (PBS) solution. The refractive index of the liquids was determined by a conventional Abbe Refractometer (Müller, Germany) with a precision of 1 × 10^{-4} RIU.

Results and discussion

The rolled-up optofluidic ring resonator

The integrated glass microtubes not only act as microfluidic channels but also as optofluidic components, constituting the sensor of the chip. We adapted a U-shape design of the patterned layer rolled-up into a microtube with three windings (Fig. 2a–c), similar to that reported by Strelow *et al.*,[25] to enable a good optical confinement along the tubular axis.

Fig. 2d shows PL data acquired from the central position of a RU-OFRR. The spectrum reveals eight groups of modes, each of them corresponding to an azimuthal resonant condition labeled

Table 1 Utilized liquids sorted by refractive index (RIU = refractive index unit)

Liquid	Refractive index [RIU]	Refractive index change in respect to previous liquid [10^{-4} RIU]
DI water	1.3330	—
PBS	1.3345	15
PBS + 100 mM glucose	1.3369	24
PBS + 200 mM glucose	1.3394	25
PBS + 500 mM glucose	1.3472	78

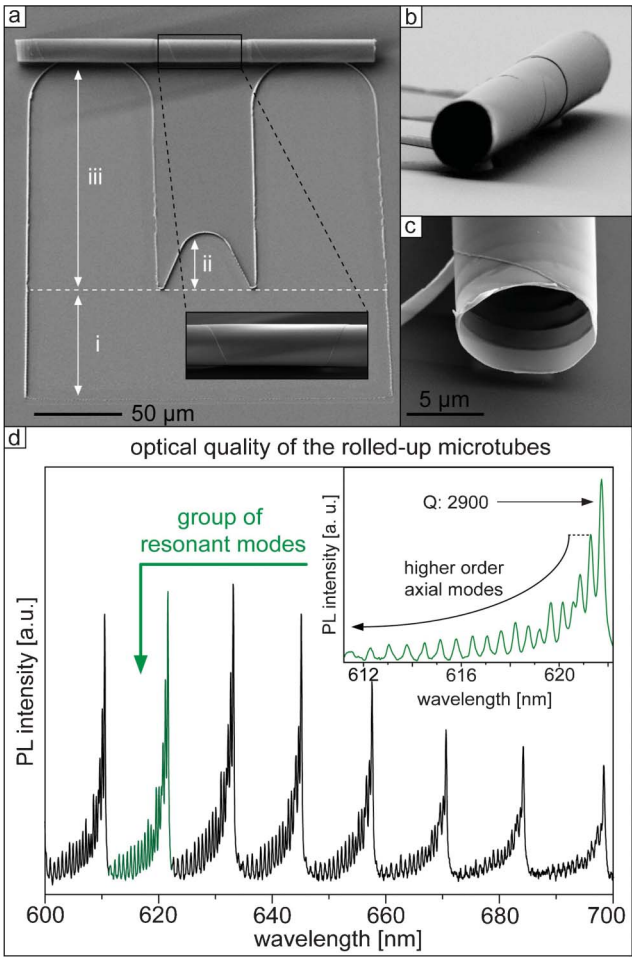

Fig. 2 Microtube fabrication and optical characterization. (a) The scanning electron microscopy (SEM) image shows a U-shape pattern and a RU-OFRR. The pattern is separated into three segments (i to iii) by the white dashed line. The inset shows a magnification of the center of the free-standing part of the microtube with an outer diameter of 13 µm. (b) Side view SEM image of a free-standing elevated rolled-up microtube. (c) Close-up of a microtube end where the compact rolling is clearly seen. (d) PL spectrum at the center part of a free-standing RU-OFRR. The inset illustrates one resonant azimuthal mode with an associated series of axial modes.

by the azimuthal mode number m.[25] The series of closely spaced modes on the short wavelength side of each azimuthal mode are higher order axial modes (see inset of Fig. 2d) and originate from the axial confinement[25] in the middle of the microtube. The mode with the highest intensity for each group of modes reaches an average Q value of 2900. This value is derived from the peak linewidth after fitting the modes with Lorentzian curves, and represents the highest value reported so far for RU-OFRRs.

Transfer of microtubes and final assembly preparation

The sockets consist of three-dimensional (3D) SU-8 structures, which include support and guidance layers into which the microtubes can be plugged. The dashed line in the optical image in Fig. 3a indicates the trench in the sockets where the transferred microtube will be placed, as depicted in the sketch in Fig. 3b. The location, orientation and number of sockets can

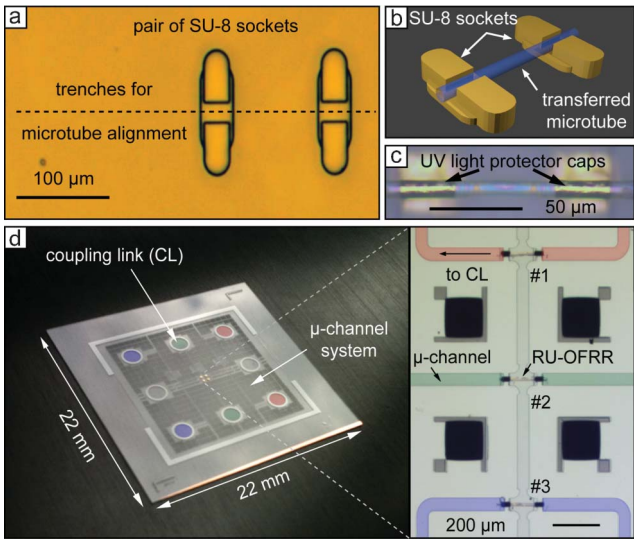

Fig. 3 Transfer, protection and integration of a microtube. (a) Optical image of a pair of SU-8 10 sockets for elevating a transferred RU-OFRR. The dashed line indicates the position of the trenches in the sockets used as alignment guides during the transfer. (b) 3D sketch of a transferred microtube placed into the socket structures. (c) Optical image of a transferred microtube with applied UV-light protector caps on top. (d) Overview of the entire chip with a microchannel system and the coupling links. The zoomed-in view depicts three labeled rolled-up OFRRs integrated into a microchannel structure. The colored channels are connected to the corresponding coupling links on the chip structure with the same color.

be chosen on demand, depending on the intended application and size of the microtubes. In this particular case, the length of the microtube is 200 µm, and therefore a distance between two sockets of 140 µm provides a stable support for the microtube. After transferring the microtubes, they are pinned to the sockets and stabilized by ALD against mechanical stress arising during the additional integration steps.[19,26]

To avoid polymerization of the SU-8 photoresist inside the microtubes after exposure by UV-light (see fabrication step 5), protector caps based on an Au layer sandwiched between Cr were deposited onto the microtube (Fig. 3c). Chromium improves the adhesion of the Au layer to metal oxides such as the Al_2O_3 layer on the substrate and the SiO_2 layer on top of the chromium. This additional SiO_2 layer provides a good adhesion to the SU-8 polymer layer applied in step 5.[27]

Microfluidic system

The microfluidic system is formed by a photo-lithographically patterned SU-8 10 polymer layer with a height of 20 µm.

The photograph in Fig. 3d shows the target microchip substrate containing defined structures such as the coupling links (CL) for the in- and outlets of the system and a microchannel system. The zoomed-in view in the Fig. 3d optical microscope image is a zoomed-in top view from the center of the substrate containing three microtubes (#1, #2 and #3) integrated into the microchannel system, which can be accessed and operated independently.

The final structure of the integrated microtube into the microfluidic channel system is schematically depicted in Fig. S1

(ESI†). The microfluidic channels and the integrated microtubes are located between the supporting glass substrate and the PDMS lid that seals the system.

Handling of liquids and sensing setup

A pressure driven flow method is utilized to drive fluids in and out of the microfluidic system. Syringes connected to a software controlled pumping system are used as an analyte-dispenser as well as an analyte-collector. The scheme in Fig. S2† shows the microfluidic set-up and a sequence of fluids pushed through a RU-OFRR. Different solutions, *i.e.* DI water, PBS and PBS with three different concentrations of glucose are used as model analytes to demonstrate the suitability of the integrated RU-OFRR as a RI optofluidic sensor. Each segment of solution of 2 μl volume is separated by 2 μl of air. Before the first liquid enters the microtube, the laser of the PL system is focused on the central part of the microtube's lobe and this position is maintained during the entire measurement. The analytes are pushed through the sensor and collected afterwards with the analyte collector syringe.

Sensor characterization

The sensing mechanism of the RU-OFRR is the response of the resonant modes to the change in RI inside the microtube. The circulating light within the tubular wall forms an evanescent field, which can interact with the volume at the distance of a few hundred nanometers inside and outside the microtube.[30] When fluids with different RIs are introduced into the RU-OFRR, the peak positions of the resonant modes change in order to maintain the resonant conditions. The change in RI is more pronounced if a gaseous phase (*e.g.* air with RI = 1.0) is replaced by a fluid (RI ≈ 1.33). An example of an optical sensing sequence of air and liquids flowing through the integrated RU-OFRR is depicted in Fig. S2.† A quantitative determination of different liquids inside the RU-OFRR can be carried out by monitoring the peak positions of the transverse-magnetic (TM) polarized modes, as illustrated by the dashed circles in Fig. S2b.†

Details of the shift and the changes in the PL spectrum are shown in Fig. 4a. The PL spectra show that without a liquid, only the TM polarized modes are confined inside the tube wall, whereas a new group of modes, identified as transverse-electric (TE) polarized modes, appear when a fluid enters the RU-OFRR.[28]

The definition of TE and TM modes for our microtubes follows the established classification from Hosoda *et al.*[29] A red shift of 11 nm after changing the microtube's content from air to DI water clearly detects the difference in the refractive indices between air ($n \approx 1$) and DI water ($n \approx 1.3330$). This large shift was reproduced by all integrated microtubes and was also confirmed by employing the analytical model of planar waveguide approximation to rolled-up tubes.[9]

According to the resonant conditions, the shift in the spectrum is not only sensitive to the RI of the materials inside and outside the microtube, but it also depends on the tubular diameter.[30] In order to probe the changes in the tubular diameter over time, we studied the stability of the signal by using a static solution of DI water inside the integrated RU-OFRR and recording the peak position of the most intense peak for each group of TM modes (azimuthal mode numbers 62, 63 and 64) by PL spectra over more than 2 h, as shown in Fig. 4b. The first measurement (time = 0 min) is set as the reference peak position for each TM group of modes (position = 0 nm). The peak positions are very stable over time and their variation in wavelength corresponds to a standard deviation σ between 0.09 and 0.11 nm, only.

We studied the stability and reproducibility of the sensor's response (peak position) when a sequence of two different liquids (DI water and PBS) flows through the RU-OFRR. For this experiment, the most intense peak of a single TM group of modes is monitored. The filling of the analyte dispenser was carried out similarly to the example described in Fig. S2.† The tubing was first filled with four segments of 2 μl PBS and then two segments of 2 μl DI water, separated by 2 μl of air. The two DI water segments are first pumped at a rate of 1 μl min^{-1}, resulting in an average peak position of 688.35 nm wavelength, as shown in Fig. 4c. According to the higher refractive index of PBS, with a difference in RI of $\Delta n = n_{PBS} - n_{DI} = 15 \times 10^{-4}$ RIU with respect to DI water, a red shift of the peak position is expected.[9]

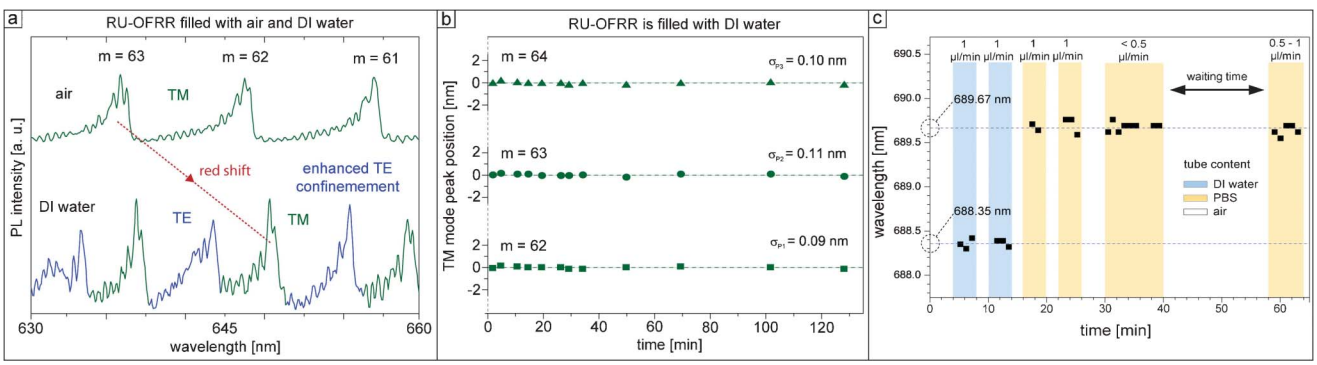

Fig. 4 Mode response and signal stability. (a) Photoluminescence spectra of the RU-OFRR with air (black line) and DI water (green line) inside the microtube. The liquid forces the resonant modes to shift to longer wavelengths and to split into TE and TM. (b) Determination of the signal stability by tracking the relative peak positions of three side by side TM modes over more than 2 h, starting with the first position as a reference. (c) In-flow detection of the resonant mode position for DI water and PBS. A subsequent sequence of two different liquids was pumped at different velocities into the RU-OFRR#1 to track the position of one resonant mode position. The average peak position for water is at 688.45 nm and the average resonant mode peak position for PBS is at 689.67 nm.

Once the RU-OFRR is filled with the flowing PBS (rate of 1 μl min^{-1}), the peak position shifts to an average value of 689.67 nm. Noticeably, the peak position is independent of the flow velocity or the delay time between each segment, proving that the optofluidic response of the RU-OFRR is stable to changes in the flow speed and the in-tube pressure, respectively.

The sensitivity S of this RU-OFRR in the RI range between DI water and PBS (Fig. 4) is calculated by the ratio between the change in the mode peak position $\Delta\lambda$ and the difference in refractive index Δn of the liquids (values taken from Fig. 4):

$$S = \frac{\Delta\lambda}{\Delta n} = 880 \frac{\text{nm}}{\text{RIU}} \quad (1)$$

This sensitivity is significantly higher than previously reported values for rolled-up ring resonators.[4,9] The relative thinness of the RU-OFRR wall (about 210 nm) with respect to the resonant wavelength causes this high sensitivity value, because it allows the evanescent field of WGM to spread outside the microtube wall.[16]

This sensitivity is significantly higher than previously reported values for rolled-up ring resonators.[4,9] The relative thinness of the RU-OFRR wall (about 210 nm) with respect to the resonant wavelength causes this high sensitivity value, because it allows the evanescent field of WGM to spread outside the microtube wall.[16]

We obtained sensitivities for different integrated RU-OFRRs ranging from 472 to 880 nm RIU^{-1}. In addition to the high optical quality of the integrated RU-OFRRs, the sensitivity is higher than previous non-integrated rolled-up ring resonators.[9,13] The corresponding detection limit (DL) for this RU-OFRR (Fig. 4) is calculated by the standard deviation of the signal stability (σ = 0.1 nm) and the sensitivity S according to:[31]

$$\text{DL} = \frac{3\sigma}{S} = 3.4 \times 10^{-4} \text{RIU} \quad (2)$$

In another experiment, fluids were pumped into the integrated sensors using the sensing sequence shown in Fig. S2a:† DI water, PBS and finally different concentrations of glucose in PBS (100, 200, 500 mM). The peak positions of the three neighboring groups of TM modes (azimuthal mode numbers m 50, 51 and 52) are monitored with respect to the RI of the fluid (data plotted in Fig. 5a). The peak position of the first fluid (DI water) is set as a reference point in all measurements. The evaluation of the linear behavior for this optofluidic sensor was performed by plotting the total shift $\Delta\lambda$ (relative to DI water) of the TM mode m = 51 *vs.* the RI of the liquid (Fig. 5b). The values of the detection limit range from 3.4 × 10^{-4} to 6.4 × 10^{-4} RIU for several integrated RU-OFRRs.

The sensor follows a linear behavior (green fit in Fig. 5b) up to a concentration of 100 mM of glucose, and saturates at higher concentrations (red dashed line).

We speculate that beyond a concentration of 100 mM the effect of glucose accumulation on the inner tubular wall deteriorates the sensing capabilities of the RU-OFRR. Our interpretation is that the glucose layer is too thick to be penetrated by the evanescent field, which is necessary for sensing. A flowing liquid can reduce the effect of material accumulation but not eliminate it. We emphasize that if we use liquids which do not alter the surface properties of the microtube wall, such as organic solvents,[9,16] the linear behaviour of the sensor may be extended to a wide range of refractive indices.

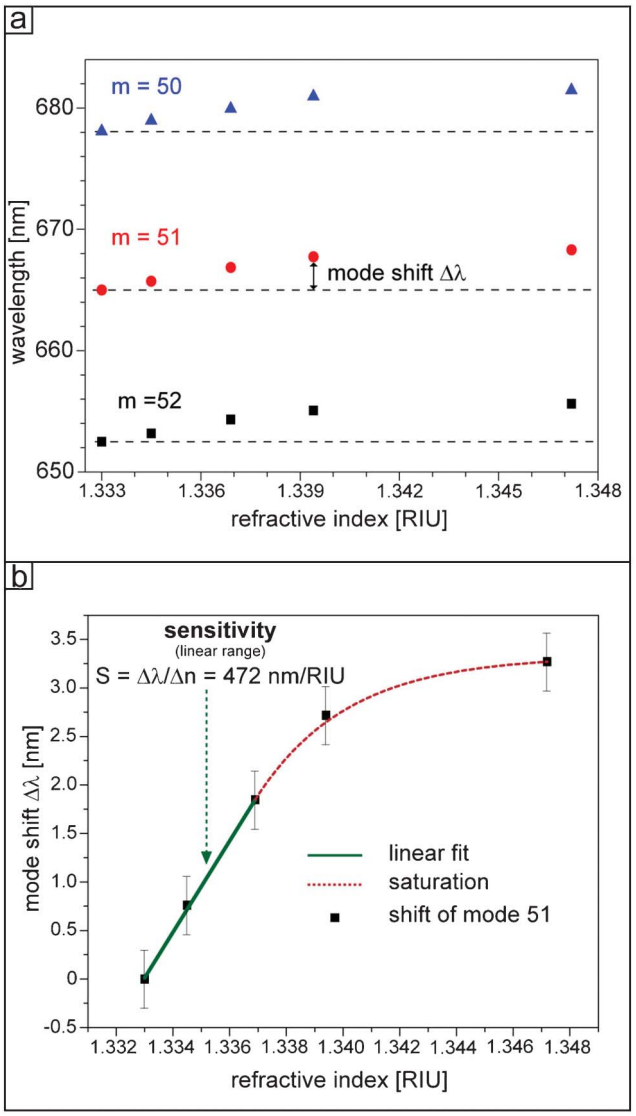

Fig. 5 Resonant mode shifts $\Delta\lambda$ for liquids with increasing refractive indices. (a) Peak position tracking of three side by side resonant modes (azimuthal mode numbers 50, 51 and 52) for liquids with different refractive indices. A higher refractive index results in a shift towards longer wavelengths for all modes compared to the initial value (dashed lines). (b) Plot of the mode shift $\Delta\lambda$ (from mode number 51) with respect to the first position (DI water). The RU-OFRR has a sensitivity of 472 nm RIU^{-1} in the linear range (green line).

Conclusions

We have demonstrated the integration of rolled-up optofluidic ring resonators with quality factors of about 2900 into microfluidic devices. The integrated RU-OFRRs can detect changes in the RI of liquids flowing through the channels with sensitivities of up to 880 nm RIU^{-1}. The optical capabilities of a single glass microtube and the integration approaches, such as the transfer of microtubes to specific locations on a microchip device, open many new applications such as label-free sensors,

integrated dye lasers or on-chip flow cytometers as stand-alone devices or additional components in existing[32] lab-on-a-chip devices.

As an example, the socket system would allow the placement, integration and combination of microtubes with different functionalities, such as rolled-up giant magneto resistant sensors[33] or rolled-up temperature controllers,[34] in order to create complex and efficient analysis devices for analytes.

Acknowledgements

This work was financially supported by the Volkswagen Foundation (I/84072 and 86 362) as well as the DFG Research Unit 1713 "Sensoric Micro- and Nanosystems". The authors thank R. Engelhard, C. C. Bof' Bufon, E. J. Smith and D. Grimm for technical support and fruitful discussions.

References

1 F. Vollmer and S. Arnold, *Nat. Methods*, 2008, **5**, 591–596.
2 I. M. White, H. Zhu, J. D. Suter, N. M. Hanumegowda, H. Oveys, M. Zourob and X. Fan, *IEEE Sens. J.*, 2007, **7**, 28–35.
3 K. Scholten, X. Fan and E. T. Zellers, *Appl. Phys. Lett.*, 2011, **99**, 141108.
4 A. Bernardi, S. Kiravittaya, A. Rastelli, R. Songmuang, D. J. Thurmer, M. Benyoucef and O. G. Schmidt, *Appl. Phys. Lett.*, 2008, **93**, 094106.
5 Y. Sun and X. Fan, *Anal. Bioanal. Chem.*, 2011, **399**, 205–211.
6 J. Hong, J. B. Edel and A. J. deMello, *Drug Discovery Today*, 2009, **14**, 134–146.
7 Y. Gao, Q. Gan, Z. Xin, X. Cheng and F. J. Bartoli, *ACS Nano*, 2011, **5**, 9836–9844.
8 F. C. Chien, C. Y. Lin, J. N. Yih, K. L. Lee, C. W. Chang, P. K. Wei, C. C. Sun and S. J. Chen, *Biosens. Bioelectron.*, 2007, **22**, 2737–2742.
9 G. S. Huang, V. A. Bolaños Quiñones, F. Ding, S. Kiravittaya, Y. F. Mei and O. G. Schmidt, *ACS Nano*, 2010, **4**, 3123–3130.
10 S. Lacey, I. M. White, Y. Sun, S. I. Shopova, J. M. Cupps, P. Zhang and X. Fan, *Opt. Express*, 2007, **15**, 15523–15530.
11 A. M. Armani and K. J. Vahala, *Opt. Lett.*, 2006, **31**, 1896–1898.
12 A. Ramachandran, S. Wang, J. Clarke, S. J. Ja, D. Goad, L. Wald, E. M. Flood, E. Knobbe, J. V. Hryniewicz, S. T. Chu, D. Gill, W. Chen, O. King and B. E. Little, *Biosens. Bioelectron.*, 2008, **23**, 939–944.
13 E. J. Smith, S. Schulze, S. Kiravittaya, Y. F. Mei, S. Sanchez and O. G. Schmidt, *Nano Lett.*, 2011, **11**, 4037–4042.
14 G. Yang, I. M. White and X. Fan, *Sens. Actuators, B*, 2008, **133**, 105–112.
15 Y. Sun, S. I. Shopova, G. Frye-Mason and X. Fan, *Opt. Lett.*, 2008, **33**, 788–790.
16 I. M. White, H. Oveys and X. Fan, *Opt. Lett.*, 2006, **31**, 1319–1321.
17 O. G. Schmidt and K. Eberl, *Nature*, 2001, **410**, 168.
18 O. G. Schmidt and N. Y. Jin-Phillipp, *Appl. Phys. Lett.*, 2001, **78**, 3310–3312.
19 G. S. Huang, Y. F. Mei, D. J. Thurmer, E. Coric and O. G. Schmidt, *Lab Chip*, 2009, **9**, 263–268.
20 S. M. Harazim, W. Xi, C. K. Schmidt, S. Sanchez and O. G. Schmidt, *J. Mater. Chem.*, 2012, **22**, 2878–2884.
21 C. Deneke and O. G. Schmidt, *Appl. Phys. Lett.*, 2004, **85**, 2914–2916.
22 D. J. Thurmer, C. Deneke, Y. F. Mei and O. G. Schmidt, *Appl. Phys. Lett.*, 2006, **89**, 223507.
23 MicroChemicals GmbH, SU-8 Datasheet, www.microchem.com.
24 Y. F. Mei, G. S. Huang, A. A. Solovev, E. Bermudez Ureña, I. Mönch, F. Ding, T. Reindl, R. K. Y. Fu, P. K. Chu and O. G. Schmidt, *Adv. Mater.*, 2008, **20**, 4085–4090.
25 C. Strelow, H. Rehberg, C. M. Schultz, H. Welch, C. Heyn, D. Heitmann and T. Kipp, *Phys. Rev. Lett.*, 2008, **101**, 127403.
26 J. W. Elam, D. Routkevitch, P. P. Mardilovich and S. G. George, *Chem. Mater.*, 2003, **15**, 3507–3517.
27 J. C. McDonald and G. M. Whitesides, *Acc. Chem. Res.*, 2002, **35**, 491–499.
28 I. M. White, J. Goring, Y. Sun, G. Yang, S. Lacey and X. Fan, *Appl. Phys. Lett.*, 2007, **91**, 241104.
29 M. Hosoda and T. Shigaki, *Appl. Phys. Lett.*, 2007, **90**, 181107.
30 X. Fan, I. M. White, S. I. Shopova, H. Zhu, J. D. Suter and Y. Sun, *Anal. Chim. Acta*, 2008, **620**, 8–26.
31 I. M. White and X. Fan, *Opt. Express*, 2008, **16**, 1020–1028.
32 S. Schumacher, J. Nestler, T. Otto, M. Wegener, E. Ehrentreich-Förster, D. Michel, K. Wunderlich, S. Palzer, K. Sohn, A. Weber, M. Burgard, A. Grzesiak, A. Teichert, A. Brandenburg, B. Koger, J. Albers, E. Neblingand and F. F. Bier, *Lab Chip*, 2012, **12**, 464–473.
33 I. Mönch, D. Makarov, R. Koseva, L. Baraban, D. Karnaushenko, C. Kaiser, K.-F. Arndt and O. G. Schmidt, *ACS Nano*, 2011, **5**, 7436–7442.
34 I. Mönch, J. Schumann, M. Stockmann, K. F. Arndt and O. G. Schmidt, *Smart Mater. Struct.*, 2011, **20**, 085016.